Bubble Dynamics and Anode Effects in Aluminium Chloride Electrolysis: Experimental and Numerical Simulation

Cong Wang[1], Tianshuo Yang[2], Hongkun Niu[3], Zhiwei Liu[4], Sen Zhou[5], Mouhamadou Aziz Diop[6] and Bingliang Gao[7]
1, 3, 4, 5. Doctoral degree students
2. Master's degree student
6. Associate professor
7. Full professor
Northeastern University - School of Metallurgy, Shenyang, China
Corresponding author: blgao@mail.neu.edu.cn
https://doi.org/10.71659/icsoba2025-al054

Abstract

This study examines anode bubble dynamics and their role in the anode effect during aluminium chloride electrolysis (ACE) using a high-temperature transparent cell. Experiments were conducted in a NaCl-LiCl-$AlCl_3$ molten salt system at 750°C with graphite electrodes. Bubble behaviour was analysed under current densities ranging from 0.4 to 2.0 A/cm^2. Results show that bubble nucleation, growth, coalescence, and detachment follow a consistent pattern. Higher current densities accelerate bubble formation and reduce detachment intervals, while increasing bubble size and gas film thickness. The anode effect is characterized by a voltage surge to about 30 V and prolonged bubble release intervals (1.4–4.5 s). Before the anode effect, bubbles detach frequently (0.07–0.6 s), but during the anode effect, a stable gas film with a "big head, small tail" morphology is formed, disrupting the current flow. These findings highlight the critical link between bubble dynamics and cell stability, offering insights for optimizing ACE to minimize energy losses. The study advances understanding of ACE as a sustainable alternative to conventional aluminium production.

Keywords: Aluminium chloride electrolysis, Bubble dynamics, Anode effect, Transparent electrolytic cell, Current density.

1. Introduction

Aluminium chloride electrolysis (ACE), proposed as a promising technical alternative to the Hall-Héroult process [1–6], has received considerable attention since its announcement by Alcoa in 1973 [7]. Meanwhile, in 1976, Alcoa established a pilot plant with an annual capacity of 15 kt/y. The ACE process offers many advantages, including excellent energy efficiency across the entire production line. The electrolysis is conducted in a closed system, thereby minimizing pollution. It operates at a low temperature (around 700–800 °C), featuring a high current density (0.8–2.3 A/cm^2), and a very small cathode-anode distance can be maintained. Chlorine (Cl_2) is the only anode product, as shown in Equation (1), and can be recycled and used for the chlorination of bauxite or alumina to prepare aluminium chloride. Therefore, the carbon anode as a non-consumable anode does not generate greenhouse gases emissions [8]. Moreover, the anode-cathode distance (ACD) can be maintained lower than in the present Hall-Héroult cell, and a bipolar stacked electrode is used, which significantly improves the voltage utilization efficiency and demonstrates remarkable potential for energy conservation.

$$2AlCl_3\,(diss) \rightarrow 2Al\,(l) + 3Cl_2\,(g) \tag{1}$$

The bipolar electrolytic cell, due to the characteristics of the electrode arrangement, effectively prevents the molten aluminium from accumulating on the cathode surface. This feature not only maintains a stable ACD but also eliminates the influence of metal movement caused by a strong magnetic field.

Hauksson and Foulkes [7] investigated voltage and current efficiency in a lab-scale electrolytic cell using graphite electrodes in the NaCl-LiCl-$AlCl_3$ molten salt at 700 °C. They systematically examined how $AlCl_3$ concentration, forced convection, electrode spacing, and current density affect current efficiency. Forced convection minimally impacted cathode polarization when $AlCl_3$ exceeded 2 wt.% but reduced diffusion control and concentration polarization at lower concentrations. Current efficiency increases sharply below 0.8 A/cm^2 but stabilizes at 80–90 % above this level. Factors such as forced convection, increased ACD, and rapid chlorine gas escape improve efficiency.

The behaviour of anode bubbles during the electrolysis process and the deposition characteristics of metallic aluminium on the graphite electrode are critical factors for ensuring stable operation of $AlCl_3$ electrolysis. Currently, there is a scarcity of studies focusing on the bubble dynamics during the aluminium chloride electrolysis process. Hence, in this study, the behaviour of anode bubbles was investigated using a transparent electrolysis cell and numerical simulations to elucidate the influence of current density on anode bubble dynamics and cell voltage.

2. Experimental and Mathematical Model

In this study, high-purity reagents were employed to ensure the reliability and reproducibility of the experimental results. The electrolyte used in the experiments was a mixture of NaCl (63.3 wt.%), LiCl (31.7 wt.%) and $AlCl_3$ (5 wt.%), which has a liquidus temperature of 650.2 °C. Electrolysis temperature is maintained at 750 °C. Sodium chloride (NaCl, 99 % purity), lithium chloride (LiCl, 99 % purity) and aluminium chloride ($AlCl_3$, 99 % purity) were fully dried to remove adsorbed moisture prior to use. The total mass of the electrolyte utilized in the electrolysis experiments was approximately 600 grams. The graphite anodes and cathodes were prepared using high-purity graphite (99 % purity) by Kejin Graphite Ltd, Shenyang, China.

A high-temperature transparent aluminium electrolysis cell (TAEC) [9], Figure 1 (a), was employed for studying the behaviour of anode bubbles in the melt. Figure 1 (b) shows the design of the side-observation transparent electrolysis cell, which consists of a two-chamber quartz crucible. The left chamber served as the anodic compartment with a dimension of 75 × 65 × 100 mm, while the right chamber functioned as the cathodic compartment with a dimension of 35 × 65 × 100 mm. The two chambers were connected by a 2-mm gap at the bottom of the middle wall, which allowed the current to flow from the anode compartment to the cathode compartment. The graphite anode had dimensions of 40 × 20 × 70 mm and featured an inclined angle of 5°. The anode was shielded by a boron nitride sleeve (as shown in Figure 1 (d)), resulting in a working anode surface area of 8.03 cm^2. The graphite cathode measured 30 × 15 × 70 mm (Figure 1 (c)). The electrolyte had a depth of 60 mm. Both the anode and the cathode were vertically immersed in the electrolyte, with depths of 40 and 30 mm, respectively.

The bubble behaviour was recorded at a speed of 60 frames per second (FPS) through a side window of the cell using a full-frame camera (Sony, Alpha7M2) equipped with a zoom lens (TAMRON, 70-300 mm F/4.5-6.3 Di III RXD). At another window of the electrolytic cell, a LED light source was utilized to capture higher-quality images. A DC power supply (IT6722A) was used to apply a constant DC current between the anode and the cathode. This power supply had a maximum power of 600 W and could simultaneously collect the cell voltage and the actual operating current. A K-type thermocouple was placed in the anode chamber to simultaneously monitor the temperature of the molten salt close to the anode, as shown in Figure 1 (b).

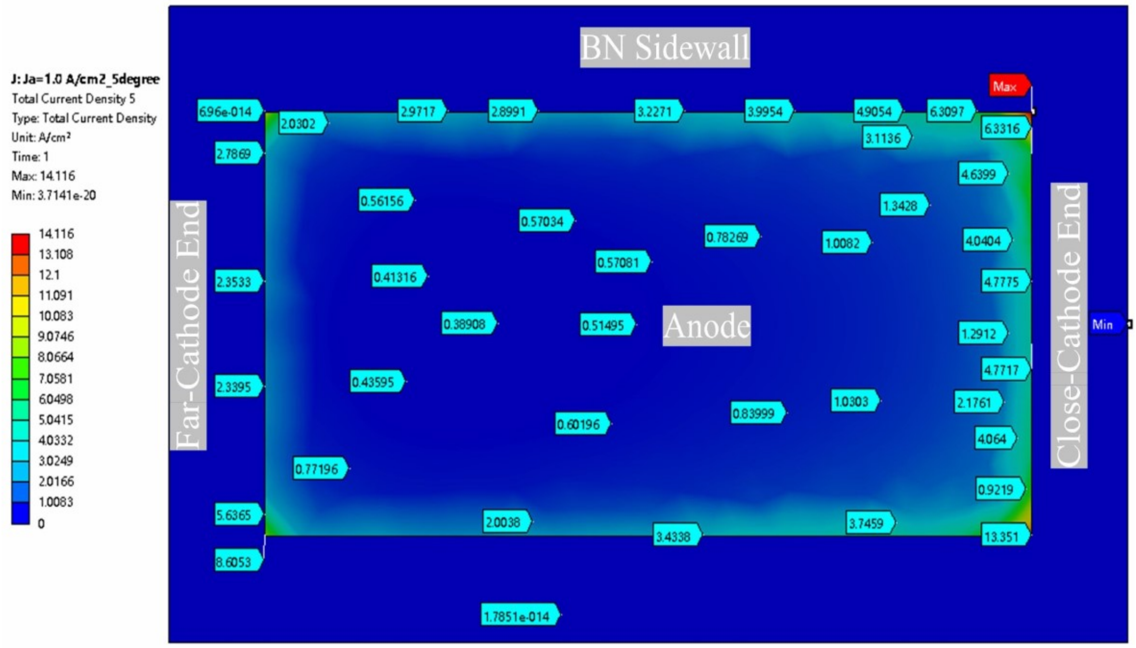

Figure 5. Simulated current density of the anode bottom surface, with an apparent current density $J_a = 1.0$ A/cm².

4. Conclusions

In this study, a high-temperature transparent electrolytic cell was utilized to directly observe bubble dynamics during the electrolysis process of $AlCl_3$ in NaCl-LiCl melts. Furthermore, the relationships between current density, bubble behaviour, and anode effects were systematically investigated. The main conclusions are as follows:

1) Under varying current density conditions, the behaviour of the bubbles at the anode bottom demonstrates consistency, including nucleation, growth, mutual coalescence, upward sliding along the inclined anode surface, further coalescence with other bubbles, and eventual detachment from the anode bottom.
2) The time interval between the detachment of large bubbles from the anode bottom is inversely proportional to the current density. Additionally, both the bubble size and the thickness of the gas film layer increase slightly with increasing anode current density.
3) During the anode effect, the cell voltage rapidly increases to approximately 30 V, accompanied by significant decline in the current. Prior to the onset of the anode effect, the release intervals for large bubbles range from 0.07 to 0.6 s; however, upon initiation of the anode effect, the intervals extend to 1.4 to 4.5 s. Numerical simulation shows the average current density at which the anode effect occurs is estimated to be approximately 4.0 A/cm².
4) Throughout the anode effect, large bubbles exhibit a distinctive morphological feature characterized by a "big head and small tail," which persist throughout the entire process.

5. References

1. Ling Ran et al., Fully-coupled electric-thermal-flow modeling and investigation of dynamic thermal-ledge behavior in aluminium electrolysis cell, *Journal of The Electrochemical Society*, 171, 2024, 093507. https://doi.org/10.1149/1945-7111/ad778f.
2. Warren E. Haupin, Principles of aluminium electrolysis, *Essential Readings in Light Metals* 2016, 3–11. https://doi.org/10.1007/978-3-319-48156-2_1.

3. Choon-Jie Wong et al., Studies on power modulation of aluminium smelting cells based on a discretized mass and thermal dynamic model, *Metallurgical and Materials Transactions B*, 54(2), 2023, 562–577. https://doi.org/10.1007/s11663-022-02709-w.
4. Guðrún Sævarsdóttir, Halvor Kvande and Barry J. Welch, Aluminium production in the times of climate change: the global challenge to reduce the carbon footprint and prevent carbon leakage, *JOM*, 72, 2020, 296–308. https://doi.org/10.1007/s11837-019-03918-6.
5. Bingliang Gao et al., Visualization of anode effect in aluminium electrolysis, *Journal of The Electrochemical Society*, 169(1), 2022, 013505. https://doi.org/10.1149/1945-7111/ac4bf5.
6. Niu Hongkun, Wang Cong, Gao Bingliang*, et al.,* A study of the passivating fluorocarbon (CF_x) film during electrochemical formation/co-evolution of CF_4 in aluminium electrolysis. *Ionics*, 30, 2024, 4811–4821. https://doi.org/10.1007/s11581-024-05635-w
7. Trausti Hauksson and Frank R. Foulkes, A study of the voltage and current efficiencies of fused salt $AlCl_3$ electrolysis using bench scale cells, *The Canadian Journal of Chemical Engineering*, 63(2), 1985, 237–243. https://doi.org/10.1002/cjce.5450630208.
8. Kai Grjotheim, A comment on the aluminium chlorine electrolyzing process for making aluminium, *Journal of Northeast Institute of Technology*, 1981, 27(2), 101–108.
9. Li Qingfeng and Qiu Zhuhan, Electrochemical Deposition of Aluminium from NaCl-$AlCl_3$ Molten Salt System. *Rare Metal Materials and Engineering*, 24(3), 1995, 59–63.
10. Hongkun Niu, Cong Wang, Bingliang Gao et al., Visualization of the impact of fluorocarbon (CF_x) passivation films and bubble layers on the anode effect, *Surfaces and Interfaces*, 2025, 59, 105968. https://doi.org/10.1016/j.surfin.2025.105968.
11. Gao Bingliang et al., Visualization of anode effect in high temperature transparent aluminium electrolysis cell, *Proceedings of the 41st International ICSOBA Conference,* Dubai, 5–9 November 2023, *TRAVAUX* 52, 1573–1580.
12. Hanno Vogel, Benedikt Flerus, Felix Stoffner and Bernd Friedrich, Reducing greenhouse gas emission from the neodymium oxide electrolysis. Part I: Analysis of the anodic gas formation, *Journal of Sustainable Metallurgy*, Vol. 3, 2017, 99–107. https://doi.org/10.1007/s40831-016-0086-0.
13. Hanno Vogel and Bernd Friedrich, Reducing greenhouse gas emission from the neodymium oxide electrolysis. Part II: Basics of a process control avoiding PFC emission, *International Journal of Nonferrous Metallurgy,* Vol. 6(3), 2017, 27–46. https://doi.org/10.4236/ijnm.2017.63003.
14. Lizhi Zhang, Xiufeng Wang and Bin Gong, Perfluorocarbon emissions from electrolytic reduction of rare earth metals in fluoride/oxide system, *Atmospheric Pollution Research*, 9(1), 2018, 61–65. https://doi.org/10.1016/j.apr.2017.06.006.